

ROBUST 3D CELL SEGMENTATION: EXTENDING THE VIEW OF CELLPOSE

Dennis Eschweiler^{1}, Richard S. Smith², Johannes Stegmaier^{1*}*

¹ Institute of Imaging and Computer Vision, RWTH Aachen University, Aachen, Germany

² John Innes Centre, Norwich Research Park, Norwich, UK

ABSTRACT

Increasing data set sizes of 3D microscopy imaging experiments demand for an automation of segmentation processes to be able to extract meaningful biomedical information. Due to the shortage of annotated 3D image data that can be used for machine learning-based approaches, 3D segmentation approaches are required to be robust and to generalize well to unseen data. The Cellpose approach proposed by Stringer *et al.* [1] proved to be such a generalist approach for cell instance segmentation tasks. In this paper, we extend the Cellpose approach to improve segmentation accuracy on 3D image data and we further show how the formulation of the gradient maps can be simplified while still being robust and reaching similar segmentation accuracy. The code is publicly available and was integrated into two established open-source applications that allow using the 3D extension of Cellpose without any programming knowledge.

Index Terms— Cellpose, 3D Segmentation, Generalist.

1. INTRODUCTION

Current developments in fluorescence microscopy have allowed the generation of image data with progressively increasing resolution and often accordingly increasing data size. 3D microscopy data sets can easily reach terabyte-scale, which requires a high degree of automation of analytical processes including image segmentation [2]. Machine learning-based segmentation approaches require annotated training data sets for reliable and robust outcomes, which often must be created manually and are rarely available. Although some resources are available for 2D, this issue is even more severe for 3D microscopy image data, since manual annotation of 3D cellular structures is very time-consuming and often infeasible, which causes the acquisition of annotated 3D data sets to be highly expensive.

2D approaches have been applied in a slice-wise manner to overcome this issue [1], diminishing the need for expensive 3D annotations, but resulting in potential sources of errors and inaccuracies. Segmentation errors are more likely to occur at slice transitions, leading to noisy segmentations, and

omitting information from the third spatial dimension, *i.e.*, a decreased field of view, leads to a potential loss of segmentation accuracy. Conversely, if there are fully-annotated 3D data sets available, robust and generalist approaches are desired to make full use of those data sets.

Stringer *et al.* proposed the Cellpose algorithm [1] and demonstrated that this approach serves as a reliable and generalist approach for cellular segmentation on a large variety of data sets. However, this method was designed for 2D application. Although a concept to obtain a 3D segmentation from a successive application of the 2D method in different spatial dimensions was proposed, the approach is still prone to the aforementioned sources of errors, missing on the full potential for 3D image data. In this paper we propose (1) an extension of the Cellpose approach to fully exploit the available 3D information for improved segmentation smoothness and increased robustness. Furthermore, we demonstrate (2) how the training objective can be simplified without loosing accuracy for segmentation of fluorescently labeled cell membranes and (3) we propose a concept for instance reconstruction allowing for stable runtimes. (4) All of our code is publicly available and has been integrated into the open source applications XPIWIT [3] and MorphoGraphX [4].

2. METHOD

The proposed method extends the Cellpose algorithm proposed by Stringer *et al.* [1], which formulates the instance segmentation problem as a prediction of directional gradients within a cell. These gradients are derived from modelling a heat diffusion process, originating at the center of a cell and extending to the cell boundary (Fig. 1, upper row). Gradients are divided into separate maps for each spatial direction, which can be predicted by a neural network alongside a foreground prediction map to prevent background segmentations. After prediction of the foreground and gradient maps using a U-Net architecture [5], each cell instance is reconstructed by tracing the multidimensional gradient maps to the respective simulated heat origin. All voxels that end up in the same sink are ultimately assigned to the same cell instance. For processing images directly in 3D and benefiting from the full 3D information, we propose multiple additions to the Cellpose approach and necessary changes to overcome memory

*Correspondence should be addressed to {dennis.eschweiler, johannes.stegmaier}@lfb.rwth-aachen.de

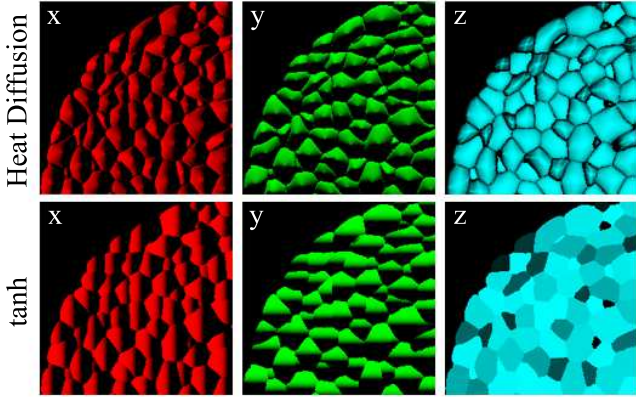


Fig. 1. Gradient map representation of cell instances in x (red), y (green) and z (blue) directions. The upper row shows heat diffusion simulations [1], while the lower row shows the simplified hyperbolic tangent distributions. Brightness indicates the gradient direction.

limitations and prevent long run-times.

We propose to use a different objective for the generation of the gradient maps, since calculation of a heat diffusion in 3D (Fig. 1, top) is computationally expensive. Instead, we rely on a hyperbolic tangent spanning between cell boundaries in each spatial direction (Fig. 1, bottom). Note that the different formulation constitutes a trade-off between lower complexity and the ability to reliably segment overly non-convex cell shapes. Predictions are obtained by a 3D U-Net [6], including all of the three spatial gradient maps for the x , y and z direction, respectively, and the additional 3D foreground map highlighting cellular regions. Since the training objective is formulated by a hyperbolic tangent, the output activation of the U-Net is set to a hyperbolic tangent accordingly. Processing images directly in the 3D space has the advantage of performing predictions only once for an entire 3D region, as opposed to a slice-wise 2D application, which has to be applied repetitively along each axis to obtain precise gradient maps for each of the three spatial directions.

Reconstruction of cell instances is done in an iterative manner, by moving each voxel within the foreground region along the predicted gradient field by a step size $\delta_{recon}(x, y, z) = g(x, y, z) * s_{recon}$, given by the magnitude of the predicted gradient at each respective position $g(x, y, z)$ and a fixed integer scaling factor s_{recon} . The number of iterations is defined by a fixed integer N_{recon} , which is adjusted by the presumed maximum cell radius r_{cell} and, thus, the maximum number of steps necessary to move a boundary voxel to the cell center. Ultimately, each voxel ends up in the vicinity of the corresponding cell center and can be assigned the respective cell label. This assignment process is based on mathematical morphology rather than applying clustering techniques. A morphological closing operation

using a spherical structuring element with a maximum radius of half the estimated average cell radius r_{cell} is applied to determine unique clusters in form of connected components. This allows for a constant and fast run-time, independent of the potentially large quantity of cells in 3D image data.

3. EXPERIMENTS AND RESULTS

To evaluate our method, we conducted four different experiments on the basis of the publicly available data set from [7]. The data set includes 125 3D stacks of confocal microscopy image data showing fluorescently labeled cell membranes in the Meristem of the plant model organism *A. thaliana*. We divided the data set into training and test sets, where plants 1, 2, 4 and 13 were used for training and plants 15 and 18 were used for testing. The test data set comprises about 37000 individual cells. Furthermore, we show how well each of the approaches performs on unseen data to assess the generalizability to different microscopy settings. Therefore, we used a manually annotated 3D confocal stack of *A. thaliana*, comprising a total of 972 fully annotated cells. Annotations were manually obtained using the SEGMENT3D online platform [8]. The experiments are structured as follows:

Baseline_{pretrained} As a baseline we used the publicly available Cellpose cyto-model and applied it to the test data set using the 3D pipeline published in [1]. Since the model was trained on a large and highly varying data set, we did not perform any further training.

Baseline_{specialized} The second experiment was designed to be a second baseline, as we used the original Cellpose approach [1] and trained it from scratch using the above-mentioned training data set from Willis et al. [7] for 1000 epochs, which we found sufficient for convergence. To reduce memory consumption and prevent high redundancies, we extracted every fourth slice of each 3D stack of the training data set to construct the new 2D training data. This experiment constitutes a specialized case of the baseline approach.

Extension_{heat} Our proposed 3D extension was first trained with the original representation of the gradient maps, formulated as a heat diffusion process [1]. The 3D U-Net was trained on patches of size $128 \times 128 \times 64$ voxel for 1000 epochs using the Meristem training data set from Willis et al. [7]. In every epoch, one randomly located patch was extracted from each image stack of the training data set. To obtain the final full-size image, a weighted tile merging strategy as proposed in [9, 10] was used on the predicted foreground and gradient maps, before reconstructing individual instances.

Extension_{tanh} For the fourth experiment, we change the representation of the gradient maps, formulated by hyperbolic tangent functions as described in Sec. 2. Otherwise, the training setup is identical to the setup of Extension_{heat}.

Final mean Dice values for the public test data set [7] are

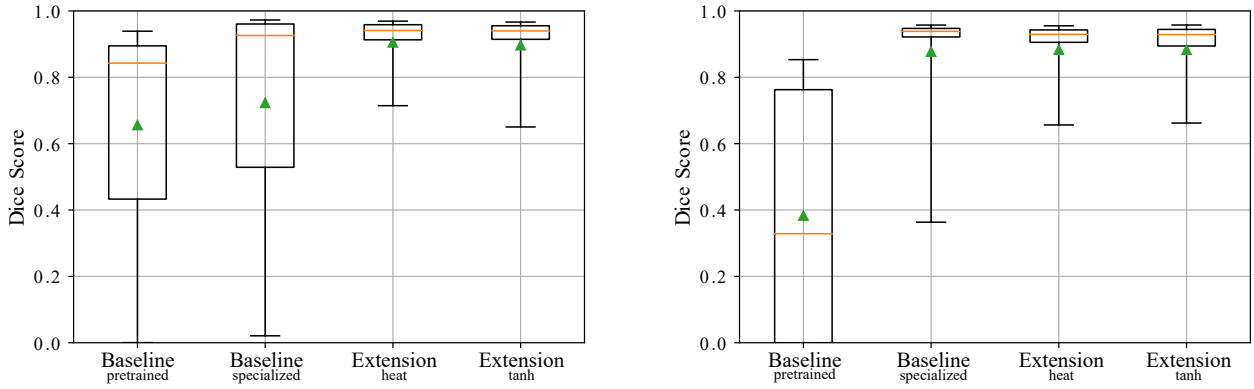


Fig. 2. Dice scores computed from segmentation results obtained for the public Meristem data set [7] (left) and for the manually annotated 3D image stack (right). The experiments include pretrained Cellpose provided by [1] (Baseline_{pretrained}), a retrained version of the original Cellpose architecture (Baseline_{specialized}), our 3D extension with the original (Extension_{heat}) and the hyperbolic tangent gradient formulation (Extension_{tanh}). Whiskers represent the 5th and 95th percentile, respectively, the box spans from the 1st to the 3rd quartile, the orange line shows the median value and the green triangle indicates the mean value.

0.656 for Baseline_{pretrained}, 0.723 for Baseline_{specialized} and 0.905 and 0.897 for Extension_{heat} and Extension_{tanh}, respectively (Fig. 2, left). Although Baseline_{specialized} benefits from specialized knowledge and shows improved segmentation scores, both baseline approaches result in poor instance segmentations in regions with low fluorescence intensity, leading to a large spread of obtained segmentation scores. The full 3D extensions, however, are able to exploit the structural information from the third dimension to successfully outline cell instances despite the low intensity. Furthermore, similar scores are obtained for both gradient formulations. Results for the manually annotated data are shown as box-plots in Fig. 2 (right) with mean Dice scores of 0.383 for Baseline_{pretrained}, 0.877 for Baseline_{specialized} and scores of 0.883 for both, Extension_{heat} and Extension_{tanh}. Results confirm that the lack of structural 3D information leads to a loss of accuracy and that both gradient formulations perform similarly well.

To further demonstrate the generalizability of the proposed approach, we generated results for the publicly available 3D image data from a variety of different plant organs in *A. thaliana* [11]. We used the model trained in Extension_{tanh} and each image was scaled to roughly match the cell sizes of the training data set in each spatial direction. Since the ground truth did not include segmentations of all cells being visible in the image data, we limited the computation of Dice scores to annotated cells. Average Dice scores (DSC) obtained for instance segmentations of each image stack range from 0.54 to 0.91 and slices of raw image data, ground truth and instance predictions are shown in Fig. 3. Despite the data set containing cellular structures never seen during training, overall results demonstrate robustness and only decline for elongated and more complex cellular shapes.

4. CONCLUSION AND AVAILABILITY

In this work we demonstrated how the concept of Cellpose [1] can be extended to increase segmentation accuracy for 3D image data. The utilization of the full 3D information and the prediction of 3D gradient maps, helps to improve segmentation of cells in regions of poor image quality and low intensity signals. Our alternate formulation of the proposed gradient maps leads to a comparable accuracy of segmentation results, while offering a lower complexity. The morphology-based approach proposed for the instance reconstruction enables the application to 3D microscopy image data independent from the quantity of captured cells. Results obtained on completely different data sets never seen during training support the claim that this approach is generalist and robust. Code, training and application pipelines are publicly available at <https://github.com/stegmaierj/Cellpose3D>. Furthermore, we integrated the approach into the existing open source applications XPIWIT [3] and MorphoGraphX [4] to make it accessible to a broad range of community members.

5. COMPLIANCE WITH ETHICAL STANDARDS

The work deals with publicly available image data for which no ethical approval was required.

6. ACKNOWLEDGEMENTS

This work was funded by the German Research Foundation DFG with the grants STE2802/2-1 (DE) and an Institute Strategic Programme Grant from the BBSRC to the John Innes Centre (BB/P013511/1).

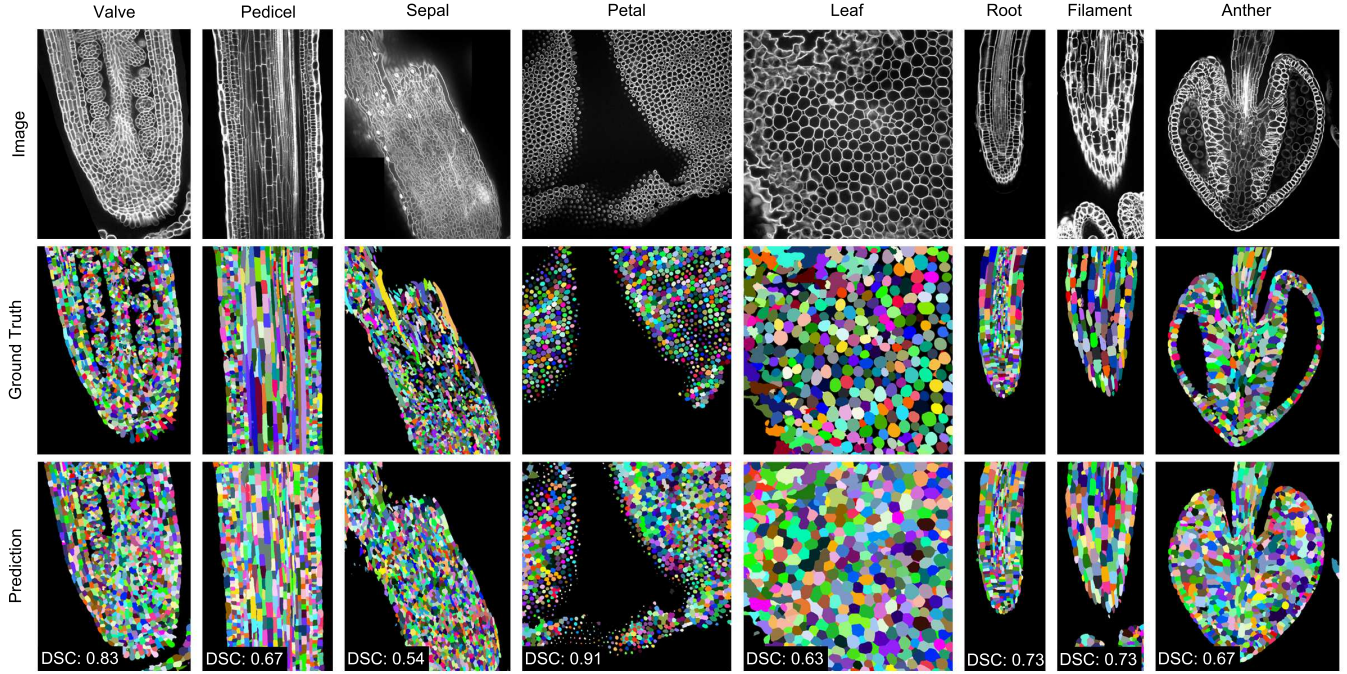


Fig. 3. Slices of raw image data (top), corresponding ground truth (center) and the predictions of the $\text{Extension}_{\text{tanh}}$ model including the obtained Dice scores (DSC, bottom) shown for different plant organs in *A. thaliana* [11].

7. REFERENCES

- [1] C. Stringer, T. Wang, M. Michaelos, and M. Pachitariu, “Cellpose: a Generalist Algorithm for Cellular Segmentation”, *Nature Methods*, vol. 18, no. 1, pp. 100–106, 2021.
- [2] E. Meijering, “A Bird’s-Eye View of Deep Learning in Bioimage Analysis”, *Computational and Structural Biotechnology Journal*, vol. 18, pp. 2312, 2020.
- [3] A. Bartschat, E. Hübner, M. Reischl, R. Mikut, and J. Stegmaier, “XPIWIT—an XML pipeline wrapper for the Insight Toolkit”, *Bioinformatics*, vol. 32, no. 2, pp. 315–317, 2016.
- [4] P. B. de Reuille, A.-L. Routier-Kierzkowska, D. Kierzkowski, et al., “MorphoGraphX: A Platform for Quantifying Morphogenesis in 4D”, *Elife*, vol. 4, pp. e05864, 2015.
- [5] O. Ronneberger, P. Fischer, and T. Brox, “U-Net: Convolutional Networks for Biomedical Image Segmentation”, in *International Conference on Medical Image Computing and Computer-Assisted Intervention*, 2015, pp. 234–241.
- [6] Ö. Çiçek, A. Abdulkadir, S. S. Lienkamp, T. Brox, and O. Ronneberger, “3D U-Net: Learning Dense Volumetric Segmentation from Sparse Annotation”, in *International Conference on Medical Image Computing and Computer-Assisted Intervention*, 2016, pp. 424–432.
- [7] L. Willis, Y. Refahi, R. Wightman, et al., “Cell Size and Growth Regulation in the *Arabidopsis Thaliana* Apical Stem Cell Niche”, *Proceedings of the National Academy of Sciences*, vol. 113, no. 51, pp. E8238–E8246, 2016.
- [8] T. V. Spina, J. Stegmaier, A. X. Falcão, E. Meyerowitz, and A. Cunha, “SEGMENT3D: A Web-based Application for Collaborative Segmentation of 3D Images used in the Shoot Apical Meristem”, in *IEEE International Symposium on Biomedical Imaging*, 2018, pp. 391–395.
- [9] T. de Bel, M. Hermsen, J. Kers, J. van der Laak, and G. Litjens, “Stain-Transforming Cycle-Consistent Generative Adversarial Networks for Improved Segmentation of Renal Histopathology”, in *Proceedings of The 2nd International Conference on Medical Imaging with Deep Learning*, 2019, vol. 102, pp. 151–163.
- [10] D. Eschweiler, M. Rethwisch, S. Koppers, and J. Stegmaier, “Spherical Harmonics for Shape-Constrained 3D Cell Segmentation”, in *IEEE International Symposium on Biomedical Imaging*, 2021.
- [11] A. Wolny, L. Cerrone, A. Vijayan, et al., “Accurate and Versatile 3D Segmentation of Plant Tissues at Cellular Resolution”, *Elife*, vol. 9, pp. e57613, 2020.